Wiss, Janney, Elstner Associates, Inc.
2941 Fairview Park Drive, Suite 300
Falls Church, Virginia 22042
703.641.4601 tel
www.wje.com

February 19, 2024

Mr. John Preiss
State Bridge Engineer
Rhode Island Department of Transportation
Two Capitol Hill
Providence, Rhode Island, 02903

Forensic Investigation of Failed Post-Tensioned Tie-Down Rods
I-195 SB Washington Bridge North (700)

Dear Mr. John Preiss:

Wiss, Janney, Elstner Associates, Inc. (WJE) has completed analysis of two post-tensioned anchor rods from Pier 7 of the southbound I-195 Washington Bridge north structure (700). The subject bridge is an 18-span structure comprised of prestressed/post-tensioned concrete multi-girder approach spans (6 west / 11 east) and a steel multi-girder main span (Span 7). There is also a three-span prestressed concrete box girder ramp to Gano street at the west end. The bridge was closed to traffic on December 11, 2023 after construction workers reported observation of a full fracture of one of the post-tensioned (PT) rods used to tie down the end spans of east and west approaches to the substructure. WJE has been engaged to perform a review of the events leading to the discovery and to evaluate the cause of the rod failures.

Site Visits

WJE personnel Michael Brown and John Cocca visited the bridge on December 16, 2023. During the site visit we observed the fractured bars in situ and the configuration and condition of the cantilever beams and structural walls at Piers 6 and 7 that the post-tensioned (PT) rods were designed to connect.

The approach structures comprise post-tensioned concrete balanced cantilever beams on concrete piers that support prestressed concrete drop-in girders between them (Figure 1). The end cantilever segments are tied down with PT rods to reinforced concrete corbels on the outward structural walls of Piers 6 and 7 to either side of the steel main span, Span 7, to counterbalance the loads of the drop-in beams in Spans 6 and 8. There are six concrete girder lines (A-F), with twin tie-down rods for each. The tie-down rods are embedded in the diaphragms at ends of the cantilever beams for girder lines B–E and extend down into the corbels, making them thus not visible for inspection. However, at the four outward corners at girder lines A and F of Piers 6 and 7, the outboard tie-down rods lie to the exterior of the cantilever beam ends, where there are no diaphragms, and are exposed from the top of the beam seat to the bottom of the concrete deck.

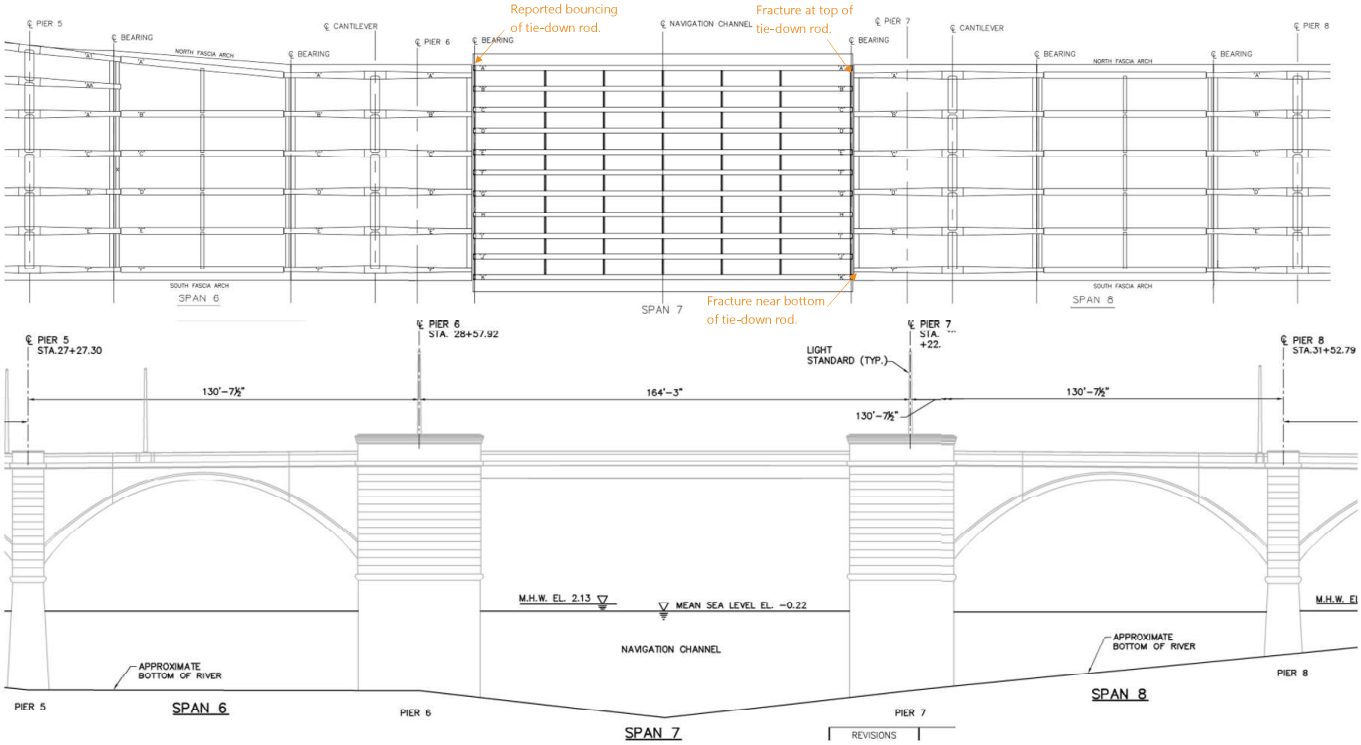

Figure 1. Framing Plan and Elevation of Spans 6 through 8, southbound I-195 Washington Bridge North (700)

During the visit, WJE observed the fractured rods at two of four corners of Span 7, at Cantilever A and Cantilever F at Pier 7. At the time, a third rod, Cantilever A at Pier 6, was suspected of also being fractured due to observed movement of the cantilever/rod, but a fracture could not be visibly confirmed. A report noted bouncing of cantilevers and gaps at bearings of adjacent girder lines at the Pier 6 and Pier 7 connections.[1]

Photos of the fractured bars taken by WJE on December 16, 2023 are shown in Figures 2 and 3. The bars were corroded on the exterior perimeter and the cross-section was reduced/tapered in the regions around the fractures. According to original design drawings, the prestressing rods were to be 1 $^{3}/_{8}$" diameter threaded high strength pre-stressing rod to be tensioned to 120,000 lbs. each (Figures 4 and 5). No specification is cited for high-strength rod and original project specifications were not provided. As a basis for comparison, Table 1 shows relative stresses based on section loss and applied post-tension load only. The applicable design specification would have limited post-tension load before losses to 0.7 f'_s.[2]

Figure 2. Pier 7 Cantilever A fractured tie-down rod

Figure 3. Pier 7 Cantilever F fractured tie-down rod

[1] VHB Visit Findings 12-11-23 (Additional Info) (Reduced).pdf

[2] AASHO Standard Specifications for Highway Bridges, 9th Ed, (HB-9), Washington, DC, 1965.

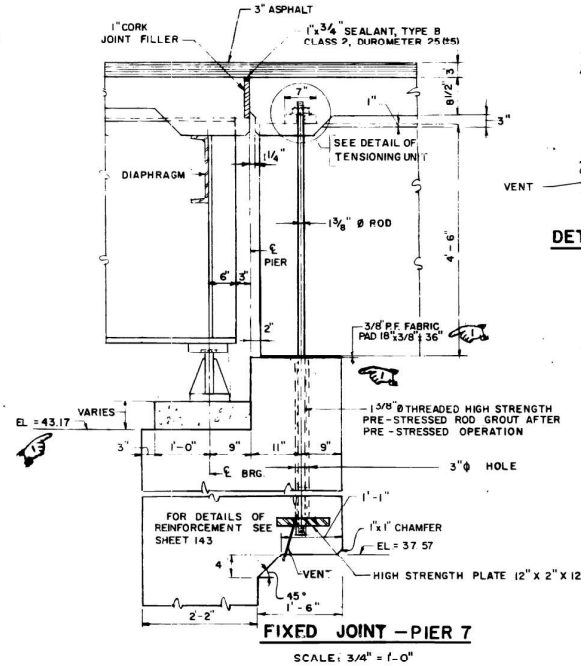

Figure 4. Section A-A excerpt from Detail Sheet 4 (Sheet 139) of original design plans (1967)

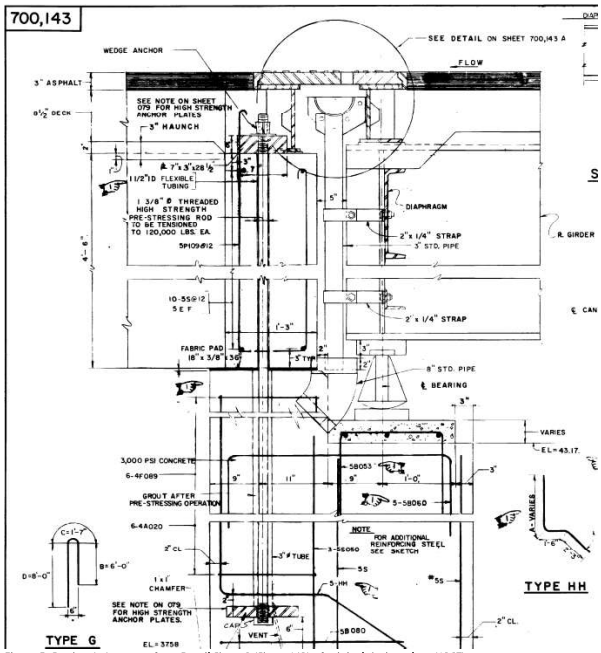

Figure 5. Section A-A excerpt from Detail Sheet 8 (Sheet 143) of original design plans (1967)

Table 1. Comparative stresses in nominal and deteriorated sections based on applied 120-kip post-tension load

Section	Diameter (in)	Area (in^2)	Stress (psi)
Nominal rod	1.375	1.485	80,814
Cantilever A rod at failure	0.996	0.779	154,018
Cantilever F rod at failure	0.904	0.641	187,169

Metallurgical Evaluation

On January 5, 2024, John Cocca returned to the site. With the assistance of the current contractor, three segments of tie-down rod containing the identified fractures were obtained. The first was a long section of rod from Pier 7 Cantilever A below the fracture. Since the fracture occurred nearly flush with concrete at the top of the rod, it was not feasible to obtain the mating top face of the fracture. The second and third segments were those below and above the fracture at Pier 7 Cantilever F. The rods were wrapped and transported for shipping to WJE's metallurgy laboratory in the Janney Technical Center in Northbrook, IL.

The PT bar segments were catalogued, measured, and photographed before being subsampled for testing and metallographic evaluation. Short segments containing the fracture surfaces at the ends of the bars were cut off for further microscopic evaluation and chemical testing. An 18-inch segment from the longer portions of both bars were removed and shipped to Product Evaluation Systems (PES) in Latrobe, PA for mechanical testing (tensile and Charpy V-notch (CVN) impact). The details of visual, mechanical, chemical, and metallographic evaluation are presented in Appendix A.

Findings

The results of the metallurgical evaluation are as follows:

- The tie-down rods were confirmed to be fabricated from chromium-alloyed, high-carbon steel with ultimate tensile strength (158.9 and 165.5 ksi) and associated elongation (10.7 and 13.5%), as well as hardness of the steel (HRC 32.1 and 34.6), all tested at room temperature.
- Toughness of the steel (3.7 and 4.3 ft-lbf) as indicated by CVN tested at 40°F is well below the requirements of modern specifications; however, impact toughness requirements for steel were not implemented in AASHTO/ASTM specifications until after this bridge was designed.
- The steel elemental composition and pearlitic microstructure are consistent with the reported material properties.
- Significant corrosion existed on both the exterior perimeter and the fractured faces of the rods. Chemical composition confirmed iron and oxygen rust product with silicon, chloride, and bromine in measurable concentrations; Thus, corrosion was likely induced by a combination of roadway deicing salts and spray from marine water sources, which is consistent with the fact the highway bridge crosses a tidal portion of the Seekonk River near Narragansett Bay.
- At the locations of fracture, bar section had been reduced to 0.986 to 1.006 inch in diameter and 0.882 to 0.925 inch in diameter for Cantilever A and Cantilever F rods, respectively. From a nominal design diameter of 1.375 inch, this represents losses of 48% and 57%, respectively, of the original cross-sectional area.

- Metallographic evaluation showed the microtopography of the fracture faces had been degraded by corrosion and the thickness of corrosion product on the fracture faces was almost half that of the remaining corrosion on the exterior perimeter of the bars.
- Observation of the pearlitic grains structure showed no evidence of plastic deformation (i.e., yielding) of the steel near the fracture surfaces and secondary cracking adjacent to the fracture surface is consistent with rapid, brittle fracture.

Conclusion

Based on the findings, WJE concludes that it is highly probable that the two cantilever PT bars evaluated for this study fractured due to tensile overstress of remaining cross-sections that had been progressively reduced by corrosion. The estimated stresses at failure based on post-tension load alone are close to or exceed the ultimate tensile strengths of the materials determined during this investigation. The substantial loss of cross section caused by corrosion combined with the steel's poor toughness limited the bars' capacity to accommodate a temporary overstress with plastic deformation and strain hardening, and thus the failure is believed to have been rapid and brittle in nature. Given the substantial loss of detail and the thickness of corrosion product on the fracture faces, it is highly unlikely that these fractures occurred within 6 months of the time the fractures were discovered. It is unclear why the bars experienced greater corrosion-induced section loss near the top and bottom concrete interfaces, but it may have been influenced by the flow and ponding of chloride-contaminated runoff through joints from the deck above and may also have been influenced by moisture accumulation (e.g., condensation) and concentration gradients (e.g., chloride and oxygen) along the bar surface at the concrete-to-air interface.

This study was focused on the materials properties of the samples and a metallurgical evaluation of the rods and fracture surfaces. Further evaluation of how those test results fit into our larger investigation is ongoing. WJE is continuing its investigation into the circumstances surrounding the failures and will provide our assessment of the broader factors in a separate report.

Sincerely,

WISS, JANNEY, ELSTNER ASSOCIATES, INC.

Michael C Brown, PhD, PE, FACI
Associate Principal

WJE

Mr. John Preiss
Rhode Island Department of Transportation
February 19, 2024

APPENDIX A. METALLURGICAL EVALUATION

Wiss, Janney, Elstner Associates, Inc.
330 Pfingsten Road
Northbrook, Illinois 60062
847.272.7400 tel
www.wje.com

February 19, 2024

Michael Brown
Associate Principal
WJE

Evaluation of I-195 Washington Bridge PT Bar Fractures
WJE No. 2023.7858.0

Metallurgical Evaluation

Two PT bars identified as being from Cantilever A and Cantilever F were received by WJE Metallurgy on January 17, 2024. The Cantilever A sample was a single length with a fracture face at one end. Cantilever F was received in two pieces that had mating fracture faces, which WJE labeled as Cantilever F-Top and Cantilever F-Bottom. The purpose of the metallurgical evaluation was to determine the failure mechanism(s) and most probable root cause of the two failures.

Visual Examination

The received bars were approximately 4 feet (Cantilever A) and 2 feet 5 inches (Cantilever F) in length (Figure 1). The surfaces of both bars were reddish-brown and uniformly rusted. Each end of Cantilever A appeared tapered, one side to a cut surface and the other side to a fracture face. The reduction in diameter was measured on each side and is shown in Figure 2. Two diameter measurements were made 90 degrees apart on each side. The two orthogonal diameter measurements adjacent to the fracture face were 0.986 inch and 1.006 inch, while similar measurements away from the fracture face were 1.357 inch and 1.340 inch. Cantilever F also exhibited a tapered end at the fracture face. Similarly, two diameter measurements were made 90° apart adjacent to the fracture and away from the fracture (Figure 3). The diameter measurements adjacent to the fracture were 0.925 inch and 0.882 inch, and the diameter away from the fracture was 1.298 inch and 1.270 inch.

The fractured ends were sectioned from the bars for closer visual examination (Figure 4). All three fracture faces were heavily corroded, with no discernible features other than the general location of the fracture origin and the direction of fracture propagation. After chemically removing the rust from the Cantilever A fracture face, examination with the aid of a stereo zoom microscope indicated that the microtopography had been badly degraded by corrosion. Nevertheless, the macroscopic features were consistent with sudden, rapid fracture preceded by negligible plastic deformation.

Scanning Electron Microscopy and Energy Dispersive X-ray Spectroscopy (SEM/EDS)

The fracture face from Cantilever A and the non-cleaned fracture face from Cantilever F-Bottom were examined using scanning electron microscopy with energy dispersive x-ray spectroscopy (SEM/EDS). The primary purpose of the examination was to analyze the composition of the rust for the presence of any chemical species that could have accelerated the corrosion rate. EDS produces a spectrum of

characteristic x-ray energy peaks whose relative heights provide a semi-quantitative analysis of the composition. The following elements were identified in each sample: oxygen (O), bromine (Br), silicon (Si), chlorine (Cl), calcium (Ca), iron (Fe), and trace amounts of zinc (Zn), phosphorus (P), sulfur (S), potassium (K), chromium (Cr), and manganese (Mn). Table 1 summarizes the samples examined and the chemical species identified. SEM images and their respective EDS spectra are shown in Figure 5 and Figure 6.

Table 1. Qualitative Summary of Chemical Species Identified by EDS on the Fracture Face and Exterior of PT Bar Adjacent to Fracture Face

Location	O	Zn	Na	Mg	Br	Si	P	S	Cl	K	Ca	Ti	Cr	Mn	Fe
Cantilever A Fracture	XX				t	X			X		t		t	t	XX
Cantilever A Exterior of Bar	XX	t	t		t	X		t	X	t	X	X	t	t	XX
Cantilever F-Bottom Fracture	XX	t	t	t	X	X	t	t	X	t	X			t	XX
Cantilever F-Bottom Exterior of Bar	XX		t	t	X	X		X	X	t	X	t	t	t	XX

XX = abundant, X = present, t = trace amount

Analysis of Chemical Composition

Chemical analysis was performed on each cantilever bar using optical emission spectrometry (OES), approximately one inch from the fracture face. The results of the analyses, as listed in Table 2, indicated that both bars had been made from a chromium-alloyed high-carbon steel.

Table 2. Elemental Composition of Each Cantilever Bar in Weight Percent

Element	Cantilever A	Cantilever F
Carbon	0.69	0.66
Manganese	1.04	1.27
Phosphorus	0.015	0.015
Sulfur	0.028	0.025
Silicon	0.23	0.29
Chromium	0.99	1.11
Nickel	0.06	<0.05
Copper	<0.05	<0.05
Aluminum	0.04	0.04

Metallographic Examination

One longitudinal diametral section bisecting the fracture origin was taken through the fracture face of Cantilever F-Top, as indicated by the dashed yellow line in Figure 4, and prepared for metallographic observation. A metallographic montage of the entire unetched section is shown in Figure 7. Figure 8

shows the origin location and associated corrosion products, and Figure 9 shows extensive subsurface secondary cracking approximately two-thirds of the diameter away. Figure 10 shows another metallographic montage across the diameter of the fracture face, with rust thickness measurements along the sides of the bar and the fracture face. The average rust thickness along the fracture face was calculated as 0.085 mm (2.56 mil) and along the sides of the bar was calculated as 0.153 mm (6.02 mil).

The polished section was etched with 2% nital to reveal the microstructure of the PT bar, which was found to consist of fully pearlitic, equiaxed grains throughout, and was consistent with the chemical composition of the steel. A metallographic montage in Figure 11 shows the entire section in the etched condition. No macro- or microstructural evidence of tensile plastic flow was observed anywhere in the section. More highly magnified images show the pearlitic structure and corrosion at the origin (Figure 12), and subsurface secondary cracking approximately two-thirds of the diameter away (Figure 13). For purposes of comparison with Figure 11, Figure 14 shows an example of metallographic evidence, in an unrelated case, of pre-fracture tensile plasticity.

The polished section was also analyzed by EDS to characterize the elemental makeup of the corrosion along the fracture face. An elemental map at the origin is displayed in Figure 15, showing the makeup of the corrosion to be primarily oxygen and iron (rust). Some manganese sulfide inclusions were also picked up by the mapping. An elemental map was also made at the subsurface secondary cracking adjacent to the fracture (Figure 16). Similarly, the corrosion along the fracture face primarily consists of oxygen and iron. Oxygen and iron were also the primary makeup of the observed secondary cracking. Bromine was also observed in the secondary cracks and in the fracture face deposit.

Mechanical Properties

Sections of each bar were sent to Product Evaluation Systems (PES) in Latrobe, PA for tensile testing and Charpy V-notch (CVN) impact testing per ASTM A370. Hardness was also tested by WJE in the Rockwell hardness C scale in accordance with ASTM E18. The test results are listed below in Table 3.

Table 3. Mechanical Testing Performed by PES and WJE

Property	Cantilever A	Cantilever F
Average Absorbed CVN Energy (ft-lbf) at 40 °F	3.7	4.3
Ultimate Tensile Strength (UTS) (ksi)	158.9	165.5
Yield Strength (ksi)	142.0	134.9
Elongation Increase (%)	10.7	13.5
Reduction of Area (%)	26.6	37.0
Average Mid-Radius Hardness (HRC)	32.1	34.6

Discussion and Conclusions

The uniformly pearlitic microstructure, measured hardness levels below 35 HRC, and UTS values below 166 ksi, all make hydrogen-assisted cracking (HAC) an unlikely precursor to failure in this case. The two cantilever PT bars most likely fractured due to tensile overstress of remaining cross-sections that had been progressively reduced by corrosion to areas roughly 52 and 43 percent of their original values. It should

be noted that the current RIDOT bridge design manual requires essentially all bridge components to meet the AASHTO minimum CVN energy for Temperature Zone 2, which applies to service temperatures between 0 and –30 °F.[1] Steel components in Zone 2 service must exhibit a minimum average of 15 ft-lbs in CVN tests performed at 40 °F. With average absorbed energies by Cantilever A and Cantilever F of 3.7 ft-lbf and 4.3 ft-lbf, respectively, the PT bars do not meet current minimum AASHTO requirements for CVN energy in Temperature Zone 2. These impact toughness provisions were generally introduced by AASHTO between 1968 and 1974, and thus were not applicable at the time the bridge was designed.[2] The role of the steel's poor toughness was to limit the bars' capacity to accommodate a temporary overstress with plastic deformation and strain hardening. This translates to the PT bars having had limited capacity for pre-fracture deformation, meaning that a tensile failure would likely exhibit little to no plastic deformation prior to fracture. The observed secondary cracking subjacent to each fracture face is also consistent with rapid brittle fracture, due to the common tendency of running brittle fractures to exhibit crack-tip branching.

Based on rust layer thickness on the fracture faces, it is highly likely that the fractures occurred prior to the most recent bridge inspection six months ago. In the reduced sections where fracture occurred, the absence of observable plastic flow in the pearlitic steel microstructure suggests that the loss of section was primarily due to corrosion rather than pre-fracture tensile necking. The sodium (Na), calcium (Ca), chlorine (Cl), and bromine (Br) detected in the corrosion products suggest the presence of sodium and calcium chloride salts (with bromide impurities) commonly used in roadway deicing. However, the strength of the bromine peaks in the EDS spectra indicate that the primary source of the salt deposits may have been sea spray, since the ratio of bromide ions to chloride ions is more than an order of magnitude higher in seawater than in solutions of deicing salts. In the present case it would be reasonable to conclude that both sea spray and deicing salts were involved. More importantly, salt-bearing moisture from any source is well known to accelerate the aqueous corrosion of steel.

Sincerely,

WISS, JANNEY, ELSTNER ASSOCIATES, INC.

David C. Schmit
Associate II

Robert W. Warke, P.E.
Associate Principal

---

[1] AASHTO LRFD Bridge Design Specifications, Ninth Edition, LRFDBDS-9, American Association of State Highway and Transportation Officials, Washington, DC, 2020.

[2] Ocel, J., "Historical Changes to Steel Bridge Design, Composition, and Properties", FHWA-HRT-20-020, Federal Highway Administration, U.S. Department of Transportation, McLean, VA, January 2021.

Figure 1. As-received photograph of received cantilever PT bars.

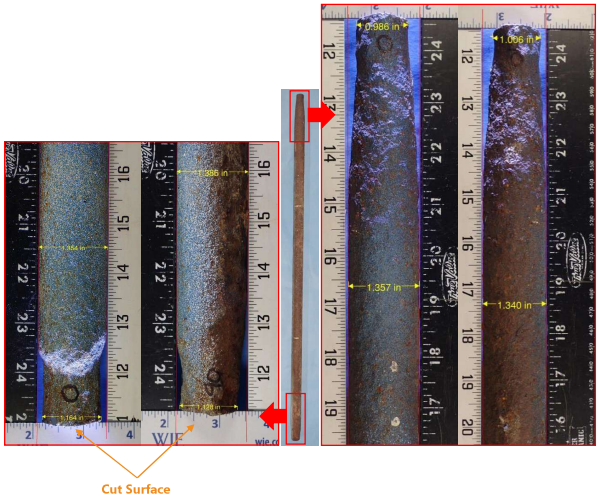

Figure 2. Cantilever A diameter measurements mapped to location on PT bar.

Figure 3. Cantilever F diameter measurements mapped to location on PT bar.

Figure 4. Fracture faces of each PT bar with labeled origin and side lighting. Note the Cantilever A fracture face has blue paint specks across the fracture face.

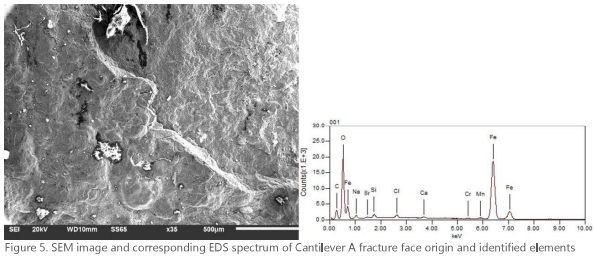

Figure 5. SEM image and corresponding EDS spectrum of Cantilever A fracture face origin and identified elements present.

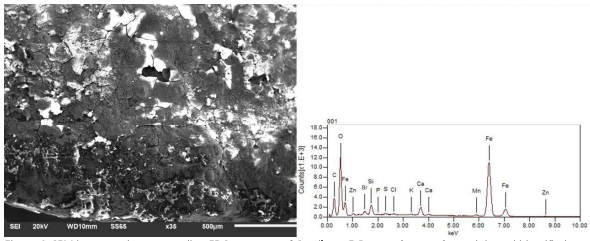

Figure 6. SEM image and corresponding EDS spectrum of Cantilever F-Bottom fracture face origin and identified elements present.

Figure 7. Cantilever F-Top: metallographic montage of an unetched diametral section through the fracture face and bisecting the fracture origin, as noted in Figure 4.

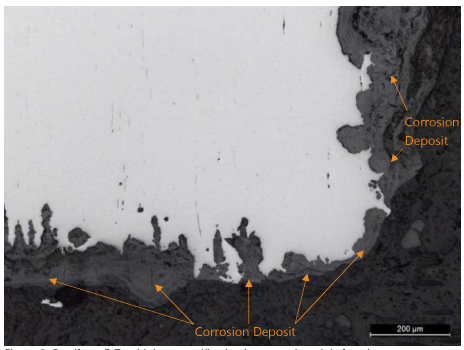

Figure 8. Cantilever F-Top higher magnification image at the origin location.

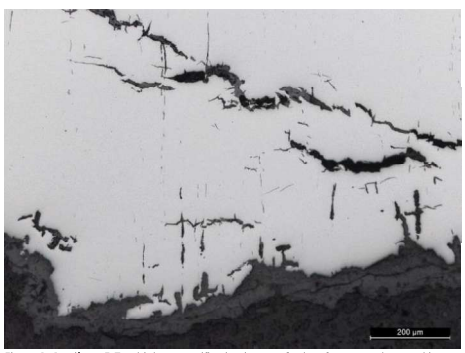

Figure 9. Cantilever F-Top higher magnification image of subsurface secondary cracking near the fracture face.

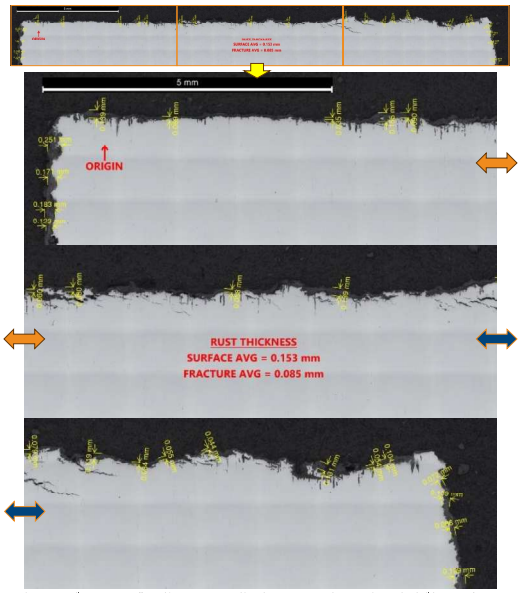

Figure 10. Cantilever F-Top metallographic montage cropped into three segments to show corrosion product buildup across fracture diameter, annotated with rust deposit thickness measurements

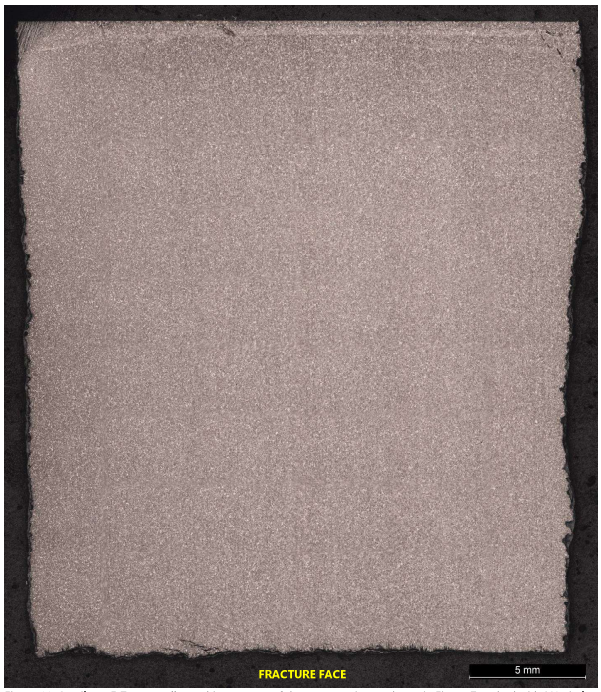

Figure 11. Cantilever F-Top: metallographic montage of the same section as shown in Figure 7, etched with 2% nital to reveal grain structure. Note the absence of tensile plastic flow in the microstructure, consistent with brittle fracture following negligible pre-fracture deformation.

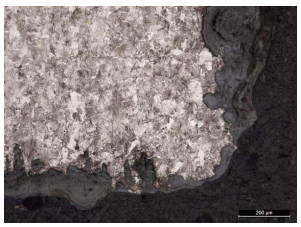

Figure 12. Cantilever F-Top: higher magnification image of etched microstructure at the origin location indicated in Figure 11.

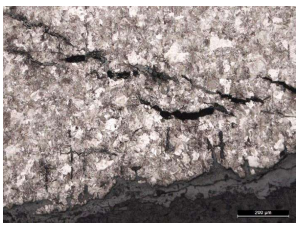

Figure 13. Cantilever F-Top: higher magnification image of the etched microstructure at the subsurface secondary cracking visible near the fracture face in Figure 11.

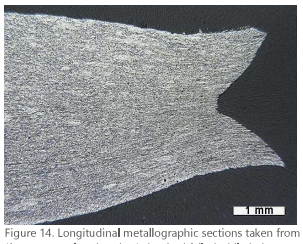

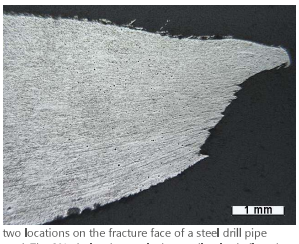

Figure 14. Longitudinal metallographic sections taken from two locations on the fracture face of a steel drill pipe (from an unrelated project) that had failed while being retracted. The 2% nital etch reveals the tensile plastic flow that preceded ductile fracture.

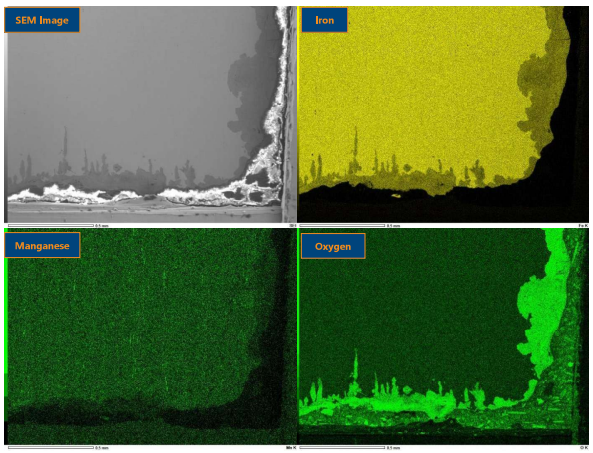

Figure 15. SEM image and EDS elemental mapping at the fracture origin of the mounted sample of Cantilever F-Top.

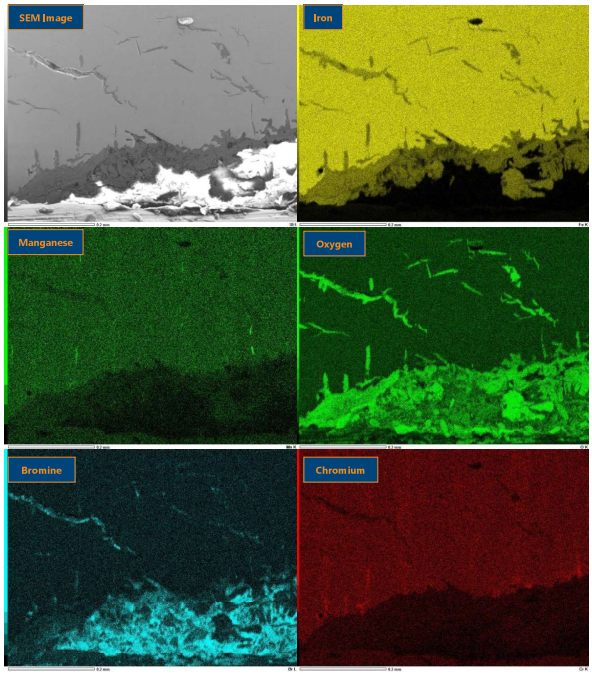

Figure 16. SEM image and EDS elemental mapping at the fissuring at the fracture face of Cantilever F-Top.